INVESTIGATION OF HEAT TRANSFER AND FLUID FLOW BEHAVIOR IN PLASMA ARC WELDING PROCESS USING FINITE ELEMENT BASED NUMERICAL MODEL

[1]Dr.Vodnala Veda Prakash,[2]Mr. S Suresh,[3]Mr. BachewalVenugopal
[123]Assistant Professor
Department Of Mechanical Engineering
Kshatriya College of Engineering

ABSTRACT

The keyhole welds are produced by the use of highconstrictedarcof plasma arc joining operation. Although, keyhole stability is one the major issue which will determine overall stability of the joining process and weld integrity. In the current article, a 3D model is developed to examine the effect of process parameters and investigate the flow behavior in the melt pool during joining operation. In the present analysis, ANSYS-WORKBENCH environment is utilized to develop a 3D physical model of the specimen. Thereby, the3D model is imported into commercial Computational Fluid Dynamics (CFD) solver ANSYS-FLUENT 15. The CFD is based on Finite Volume Method (FVM) which will discretize the whole domain into smaller elements andcompute the governing equations and different boundary constraints. A Gaussian distributed double ellipsoidal heat source model is used for simulation of plasma arc welding process. The classical constraint of physical process involved during welding is replaced by a well-defined double ellipsoidal volumetric energy source of Gaussian distribution along with different fluid flow forces such as surface tension, buoyancy,Marangoni stress, Electro Magnetic Force (EMF) and gravity. The velocity filed, temperature distribution and geometrical features of weldment is computed from the computational model and evaluated against experimental data. And, a fair agreement was achieved between experimental and numerical model.

Keywords: Thermal and Fluid Flow Modeling,Double Ellipsoidal Volumetric Heat Source, Marangoni Force, Buoyancy Force, Stereo Microscope

Introduction

Plasma arc welding (PAW) is first introduced in early 1960s by Dr. R. M. Gage. It is incorporated with micro-plasma and other high current applications. The function of PAW is

a similar to TIG welding whereby high constricted arc is formed between tungsten electrode and work-piece for joining metals of different ranges.

A non-consumable tungsten electrode is placed inside the welding torch which gives a constrained arc. The plasma arc generation is from apointed electrode which is placed inside the torch and it isindependent of shielding gas nozzle. The pilot arc is generated with assistance of a high frequency generator which is transferred to the work-piece and water cooled copper nozzle is employed for plasma arc welding. This process works with a transferred arc which is referred as Plasma arc.

In PAW, plasma gas is insufficient to shield the metal specimen during welding therefore, employment of shielding gas is a necessity to eliminate surface and other weld defects. The most commonly employed shielding gases are Helium or Argon. The plasma arc is highly constricted but it expands slightly with increasing arc length. Moreover, there is high thermal energy input and momentum transfer due to strong action of plasma arc. This in effect melts the metal specimen immediately and melt pool is formed.
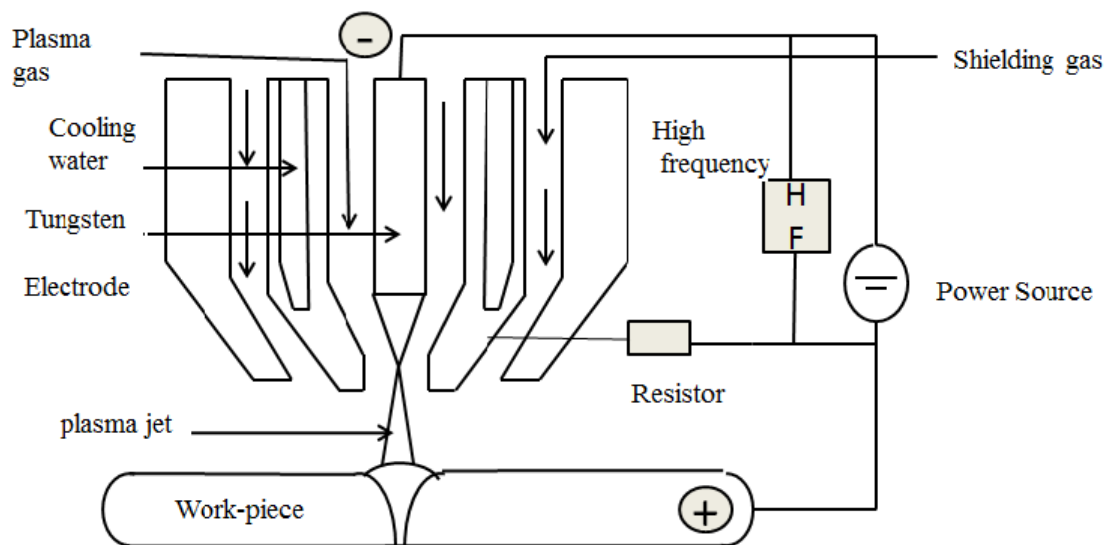

Figure 1. Schematic of PAW process.

In PAW, plasma is a group of freely flying negatively charged fast-moving electrons, neutral atoms and slow-moving positively charged ions. Due to electron and ions balance, plasmas become neutral and conduct electricity similar to metal. Electron avalanche takes place by reason of high electric field or high frequency current. Figure 1 depicts the schematic of PAW process.

Plasma torch makes PAW different from other welding process. It works like a little rocket engine. Arc is constricted due to its jet diameter and constrict degree is enhanced as the low pressure orifice cools down which makes the outer layer of the arc. And, the current

density is enhanced once the size of arc column is reduced. It is essential to be more compatible in size and shape in order to access the difficult welding location. Although,size is always dependenton the type of cooling process either water cooled or air cooled.
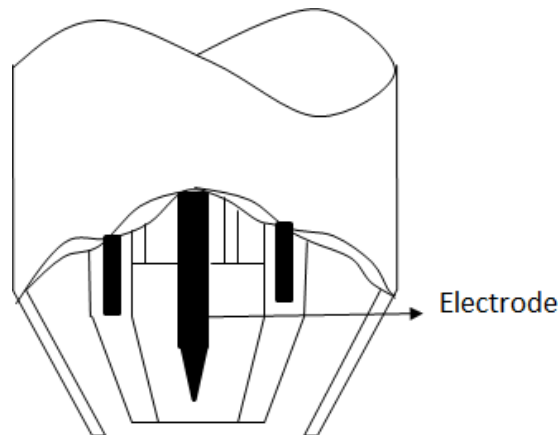
Figure 2. Schematic of Plasma torch.

Plasma arc welding can be carried out through two different approaches viz.melt-in mode and keyhole mode.Incaseof melt-in or conduction mode the plasma arc have higher ability to penetrate throughthe melt pool. As a result, a through passage is produced during the action in the weld region then it is referred as keyhole and the process is defined as key-hole mode. High heat intensity of the plasma arc creates deep and narrow pool. Initially keyhole is produced however, it is maintained by the plasma arc pressure. Key-holing is possible only with proper combinations of plasma gas flow, the travel speed of welding torch and welding current. If the plasma arc power is not high enough to penetrate through the work-piece then the joining procedure follows melt-in mode or conduction mode. Melt-in mode welding operatesbetween 15-40 Amperes while keyhole mode operatesathigher plasma forming current viz. more than 400 Amperes.The schematic of plasma torch is presented in Figure 2.

The quality of keyhole mode weldments greatly relies on the stability of the keyhole which in effect relies on heat transmission process and flow behavior inside the melt pool. Although several parameters influences the keyhole dynamics. One such measure is modification of PAW equipment for improvement of arc attributes and avoiding defect formation in real time by sensation and control. Moreover, there is a dynamic interaction of keyhole with physical process viz. flow pattern of molten metal and heat transmission during welding process. Primarily, the keyhole is surrounded by the molten metal and the gravity at any point in the molten metal is a direct function ofheight and density of the molten metal

above it. And, it is essential to prevent atmospheric contamination of molten metal under bead.

Various methods are employed to monitor keyhole process in PAW. To evaluate the electrical potential of plasma efflux, a sensor is used at the work piece exit known as efflux plasma charge sensor. Thissensor has high reliability when compared with sound signal based sensors since it is easily influenced by the environmental noise. It has simple structure and low cost. And, to visualize the melt pool and keyhole formation simultaneously from the work-piece underside an ultra-high shutter speed vision system is employed. Similarly for identifying keyhole formation from the specimenunderside, Liu et al. developed a vision system that is efficient [1].

PAW has wide range of application due to high quality weld attributes and characteristics and minimal physical and metallurgical defects [2] in robotics, aircraft, aerospace industries and automotive industries. Plasma arc welding is used to make both keyhole and non-keyhole type of weld but in this project we are concentrating on keyhole plasma arc welding.

Heat Conduction and Transport Phenomenon in PAW

The arcjoining processis a complex phenomenonsince, it involves several integrated physical forces during the process. Moreover,it is difficult to analyse the energy generation, its distribution over the specimen and its impact on fluid flow pattern during the actual joining process. Therefore, in computational modeling the energy distribution from arc to specimen is replaced by a mathematical function to approximate the actual distribution and such mathematical functions are defined as heat source models.These are employed to compute and analyse thermal and fluid flow associated problems in welding operations.

Numerical Heat transfer model

The application of energy representation through mathematical models during PAW processareanalysing keyhole formation and its characteristics. These thermal energy source models should represent the original heat source distribution. The mathematical representation of energy sources likewise disc, semi-ellipse,spherical, conical, double ellipsoidal or aunion of these modelsare mapped with geometric profiles of weldment. Infact, a relatively complex solution process is evolved due to fluctuation of temperature at designated locations. Many Researchers has proposed different effective heat source model. Initially Rosenthal [3] and Rykalin [4] developed line, point and plane thermal energy

modelsfor simulating fusion welding processes. And, after accounting limitations of proposed models Friedman [5] and Krutz et al. [6] introduced a new profile i.e. disc shape to represent energy allocation over the surface area
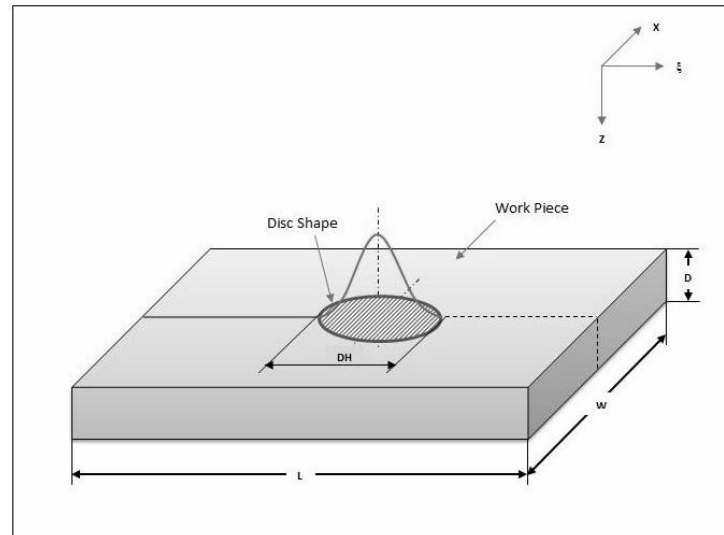

Figure 3. Schematic of disc model.

The authors presented a heat flux deposition of Gaussian distribution over the work-piecesurface. Although, it is not an adaptive option since it does not take into account theeffects of key-hole. Goldak [7] et al. proposed a double ellipsoid power density model to analyze deep penetration weld. But still it is not applicable for high density welding like keyhole PAW. Figure 3 represents adisc thermal energy source model of Gaussian distribution.Hence, a new heat source model is indeed a prior requirement to take into account the effects of keyhole of PAW process. A three dimensional volumetric conical heat source (TDC) is developed by Wu et al. [8] that consider the heat intensity distribution along the depth of the work-piece. In conical heat source model, the intensity of thermal energy source is of Gaussian function which gradually decreased along the depth of the work-piece.For keyhole stability, temperature profile is a significant factor which will govern the overall weld quality. Wu et al. [9] developed an adaptive combined volumetric power density model to incorporate heat loss from surface and higher aspect ratio of weldment.

Wu et al. [10] developed a volumetric power density model which is a combination of double ellipsoid and conic body to evaluateand analyse heat transfer and fluid flow in keyhole welds of PAW. The conic power density model considers heat intensity distribution along thespecimenthickness and it is in accordance with the thickness of conic heat source model. Although, the parameters were adjusted to demonstrate the heat transmission and fluid

flow within the melt pool.The model could imitate weldments with a higher aspect ratio and the characteristics ofplasma heat intensity. Based on conical powder density model, Li et al. [12] presented an effective composite heat source model viz. double-ellipsoidal and a conical power density models. The established model is relevant to the actual configuration of the weld and provided decent approximation in terms of temperature estimation and fluid flow distribution.

Theoretical Background

Initially work-piece is at room temperature 27^0C in the absence of preheating.Heat flux is imposed over the specimen upper surfacealong with convection and radiation heat losses while all other surfaces are insulated. It is presumed that the melted metal in the melt pool is viscous incompressible Newtonian fluid and alaminarflow pattern is followed. Different forces are considered that act on the weld pool such as buoyancy force, Marangoni shear stress and drag force. Mushy zone parameters are kept as constant during the analysis. Figure 4 describes the various forces acting in the molten pool.
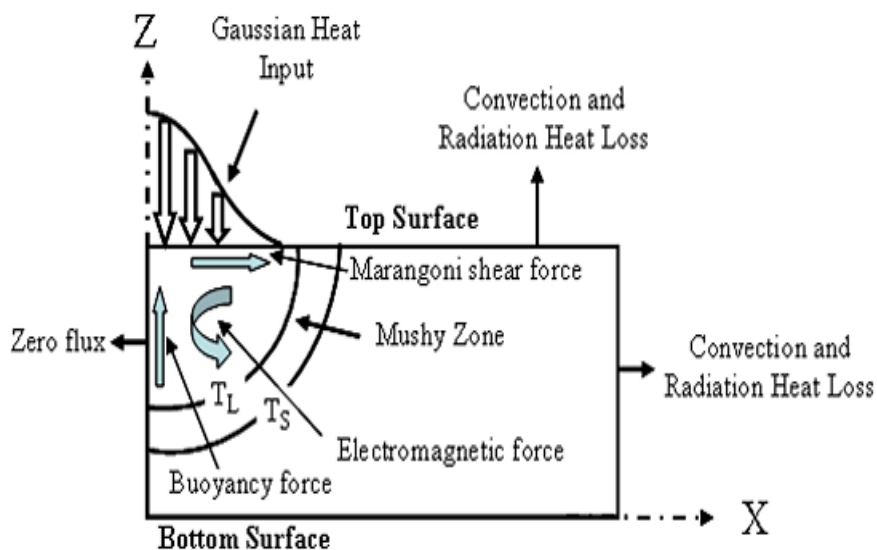

Figure 4. Forces acting on weld pool.

The following assumptions are incorporated while solving thermo-fluid analysis through computational model:

a) Laminar flow is considered and it is driven by a combination of different forces such as electromagnetic,surface tension and buoyancy forces.

b) The Gaussian distribution patternin the melt pool is followed to representcurrent density.

c) Heat loss from the boundaries of the specimen is negligible except the upper surface area.

d) The upper section of the weld is considered as flat.

For developing mathematical model for energy and fluid flow analysis the conservation of continuity, energy and momentum equations are followed[13].Themathematical formulations in three dimensional system are as follows:

Continuity equation:

$$\frac{\partial u}{\partial x} + \frac{\partial v}{\partial y} + \frac{\partial w}{\partial z} = 0 \qquad (1)$$

whereρ is density, t represents time while u, v and w denotes velocity components in X, Y and Z-axis directions respectively.

Momentum equations:

X-Momentum Equation:

$$\frac{\partial(\rho u)}{\partial t} + \nabla \cdot (\rho V u) = \nabla \cdot (\mu \nabla u) - \frac{\mu}{K}(u) - \frac{\partial p}{\partial x} - F_x \qquad (2)$$

Y-Momentum Equation:

$$\frac{\partial(\rho v)}{\partial t} + \nabla \cdot (\rho V v) = \nabla \cdot (\mu \nabla v) - \frac{\mu}{K}(v) - \frac{\partial p}{\partial x} - F_y \qquad (3)$$

Z-Momentum Equation:

$$\frac{\partial(\rho w)}{\partial t} + \nabla \cdot (\rho V w) = \nabla \cdot (\mu \nabla w) - \frac{\mu}{K}(w) - \frac{\partial p}{\partial x} - F_z \qquad (4)$$

The term P represents pressure,μ represents viscosity andF_x, F_y and F_z represent force components in X, Y, and Z-axis directions.

Energy equation:

$$\frac{\partial(\rho h)}{\partial t} + \nabla \cdot (\rho V h) = \nabla \cdot (k \cdot \nabla t) - \nabla \cdot (\rho V f_1 L_a) - \frac{\partial}{\partial t}(\rho f_1 L_a) + q(x, y, z, t) \qquad (5)$$

The influence of Marangoni stresses and surface tension are also taken into account to analyse the fluid flow. In the present analysis, Marangoni force and surface tension are considered as interfacial forces and not as body forces since, melt pool surface is considered as flat surface. The fluid dynamics within the melt pool follows conservation of momentum and continuity equations of laminar flow type[14]and mathematically the equations are represented as follows:

$$\rho \left(\frac{\partial \vec{V}}{\partial t} + \overrightarrow{V.\nabla V} \right) = -\nabla p + \mu \nabla^2 \vec{V} + S \qquad (6)$$

$$\nabla . \vec{V} = 0 \qquad (7)$$

To define the thermal enthalpy

$$H = h_{ref} + \int_{T_{ref}}^{T} C_p dt + \beta L_m \tag{8}$$

The thermal energy conservation equation is as follows

$$\frac{\partial}{\partial t}(\rho H) + \nabla.\left(\rho \vec{V} H\right) = \nabla.(k\nabla T) + S_2 \tag{9}$$

The VOF method is used by Wu et al. for tracking keyhole surface. The equation is

$$\frac{\partial}{\partial t}(\varphi \rho_2) + \nabla.(\varphi \rho_2 \vec{v_2}) = 0 \tag{10}$$

where ρ_2 and $\vec{v_2}$ are molten metaldensityand interfacialfluid velocitywhile φ represents molten metal volume with in the cell.
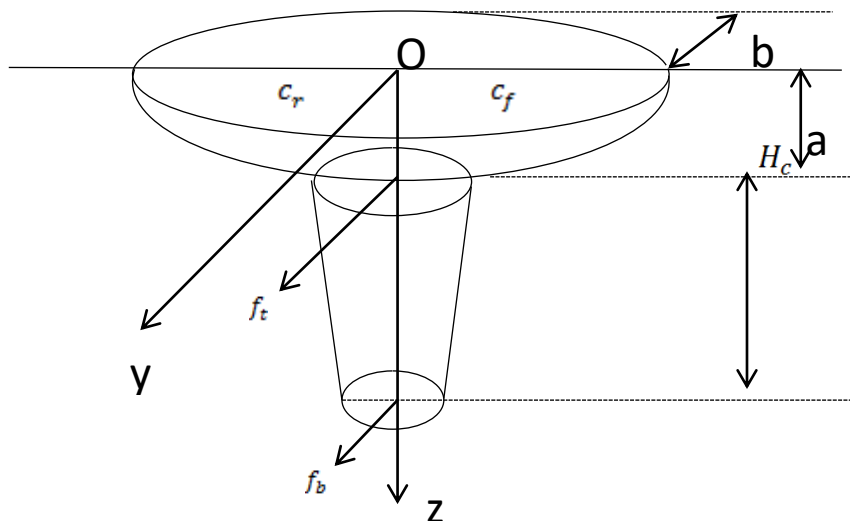
Figure 5. Schematic of combined volumetric double half ellipsoid and cone heat source model.

Figure 5schematically [15] presents the schematic of double-ellipsoidal volumetric power density model. The purpose of incorporating volumetric power density models in computational modelingis to compensate the effects of molten metal flow driven by the forces within the melt pool. From the figure it can be recognised that the rear-end section of the power density model accounts for a quadrant of one ellipsoidal while the forepart section represents another quadrant of one ellipsoid.

38

. The modelvariablesa_r,a_f, b, and cwill define double ellipsoidal power density mode. Physically, the model parameters of heat source corresponds to weld dimension that are estimated after experimental tests. The power density distribution of double ellipsoidal with arc moving along Y direction is represented as

$$q_f(x,y,z,t) = \frac{6\times 3^{1/2}\times Q_{LB}\times f_f}{a_f\times b\times c\times(\pi)^{\frac{3}{2}}} \times \frac{e^{-3x^2}}{a_f^2}.e^{-3(y-v\times t)^2/b^2}\times e^{-3z^2/c^2} \tag{11}$$

And $\quad q_f(x,y,z,t) = \dfrac{6\times 3^{1/2}\times Q_{LB}\times f_r}{a_r\times b\times c\times(\pi)^{\frac{3}{2}}} \times \dfrac{e^{-3x^2}}{a_r^2}.e^{-3(y-v\times t)^2/b^2}\times e^{-3z^2/c^2}$ (12)

wheref_f and $f_r$signifies theproportion of heat depositionat forepart and rear-end section of the double ellipsoidal. a_r,a_f, c and b are the model parameters. While v represents welding speed and t denotes time respectively. The heating and melting of the specimen is represented by anactual heat input and it is expressed as

$$Q_{LB} = \eta \times P \tag{13}$$

whereη and P signifies absorption coefficient of arc and arc power and respectively. The total summation of heat deposition proportion at front and rear section is represented by the following relation

$$f_r + f_f = 2 \tag{14}$$

Figure 6represents conical power density model. In the present analysis, r_i is defined as zero. The distribution of thermal energyat any plane that is perpendicular to Z-axis is mathematically described as [16].

$$q_v(r,z) = q_{max}\exp -\left[\frac{3\times r^2}{r_0^2\times(z)}\right] \tag{15}$$

Where q_{max} is the maximum power density, $r_o$and r presents distribution coefficient andcoordinate in radial direction. While h denotes conical power density model heightand is equal to z_e- z_0;z_e and z_0 represents upper and lower surface coordinates respectively. Thereby, the thermal energy density of conical distribution model is mathematically represented as[17].

$$q_v(r,z) = \frac{9\times P\times \eta\times e^3}{\pi\times(e^3-1)} \times \frac{1}{(z_e-z_i)\times(r_e^2+r_e r_i+r_i^2)} \times \exp\left(\frac{3\times r^2}{r_0^2}\right) \tag{16}$$

When r_0 is zero andequation (16) becomes

$$q_v(r,z) = \frac{9 \times P \times \eta \times e^3}{\pi \times (e^3 - 1)} \times \frac{1}{(z_e - z_i) \times r_e^2} \times \exp\left(\frac{3 \times r^2}{r_0^2}\right) \tag{17}$$

where P and ŋ denotes arc power and absorption coefficient.

Result and Discussion

The thermal and fluid flow analysis is performed in ANSYS-FLUENT software package which allows acquisitionof geometric features, mesh creation, different ranges of solver outputs and post-processing features.In computational modeling initially a three dimensional model is developed using ANSYS WORKBENCH 15 environment. The geometric size of the model is 120 mm × 80mm × 6 mm anda non-uniform mesh has been generated for the model.Moreover, grid convergence test has been carried out by analysing the minimum and maximum size of tetrahedron shaped cell. The geometric model of the plate and developed mesh is presented in Fig 6 and Fig 7.
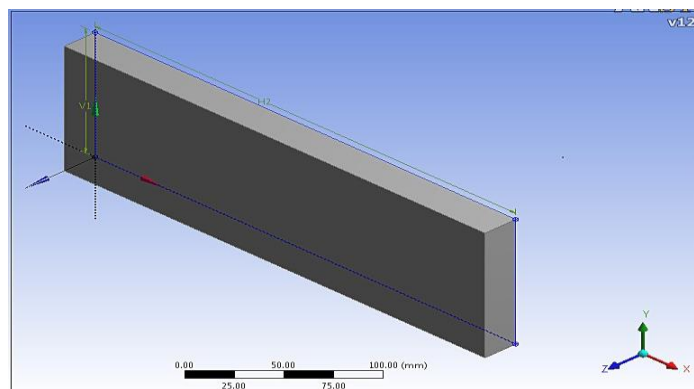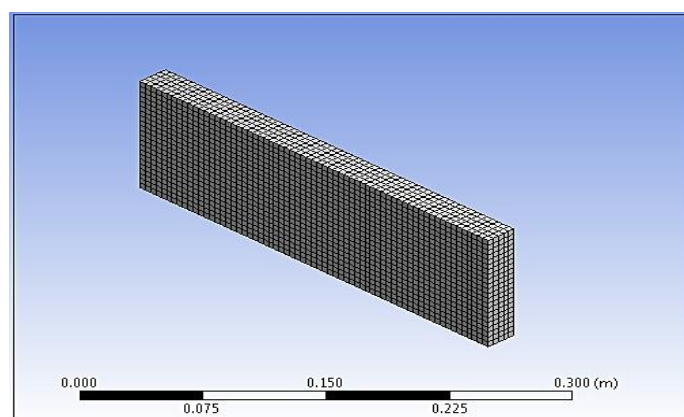

Figure 6. Geometric model of welding plate.

Figure 7. Meshing of the geometry.

Uniform structured mesh with finer grid adopted to reduce the computational time. The grids were uniformly distributed and the sizes are set as 0.2mm. Material of the model is Stainless steel 0Cr18Ni09. The thermal and physicalattributes of the specimen are linearly interpolated for the transitional temperatures. The specimen considered for computational analysis is stainless steel plate of 6mm thickness and compositional analysis of the specimen is presented in table 1.

Table 1. Compositional analysis of the 0Cr18Ni9 [1].

Elements	P	Si	Ni	Mn	Cr	S	C	Fe
Wt. %	0.035	1.0	8-11	2.0	17-19	0.03	0.08	Balanced

Table 2. The thermal and physical attributes of SS 0Cr18Ni9 [1].

Nomenclature	Value
Solidus temperature	1663 K
Liquidus temperature	1723K
Latent heat of material	2.6×10^5 J kg^{-1}
Density	7200 kg m^{-3}
Specific heat	630 J$kg^{-1}K^{-1}$
Magnetic permeability of material	1.26×10^{-6}Nm^{-1}
Radiation emissivity	0.4
Thermal expansion coefficient	$1.0 \times 10^{-4}K^{-1}$

Table 2 depict the thermal and physical attributes of parent material considered in the present work. For simulating PAW process Fluent solver is utilised and simulation result greatly depends on the input parameters and boundary conditions. The flow chart i.e. figure 8demonstrates the solution strategy for performing thermal and fluid flow analysis. Initially, user defined profile is generated for the surfaces and boundaries. In this stage, combined convection and radiation heat losses are incorporated at the upper surface and other surfaces of the substrate. Although, the surface area which is under the heat source is excluded from heat loss application. Parameters such as mushy zone parameters, buoyancy force, magnetic permeability, radiation emissivity are provided as boundary conditions based onsurfaces effects.

Table 3. Input parameters from experimental data [1].

	Condition 1	Condition 2	Condition 3	Condition 4	Condition 5
Current, I (A)	130	140	150	140	140
Voltage, (V)	19.8	21.5	21.5	21.5	21.5
Thermal efficiency of PAW	0.53	0.53	0.53	0.53	0.53
Current distribution parameter (mm)	1.22	1.22	1.22	1.22	1.22
Welding speed (mm/sec)	2	2	2	3	4

The input parameters are presented inTable 5.3. In the present analysis customized FLUENT code is utilised for computing the energy and momentum equation. Moreover, the applications and identification of heat source and other physical forces involved at preferred welding area cannot be defined in FLUENT graphical user-interface. Therefore, a user-defined function is written for heat source application and driving force involved for fluid flow over the substrate. UDF is written in Microsoft Visual studio C++ 2010 and it is compiled at the runtime

The user-defined function is available in the FLUENT graphical user interface once it is interpreted and the function code is called at every time-step.The weld center is computed based on current timewhich is mentioned in the user-defined function. The user-defined function runs on loop over each element over the substrate surface and the interval between center of each elements and the current position of the weldment is computed. Infact, if the

distance between element center is less than or equal to major or minor axis of double ellipsoidal power density model then thermal energy source is incorporated. While in case of fluid flow, if the distance between element center is less than arc radius then Buoyancy force and EMF (electro-magnetic force) are incorporated in that element. The other physical forces such as surface tension and Marangoni stresses are included in the graphical user interface by incorporating surface tension coefficient values that are dependent on temperature.
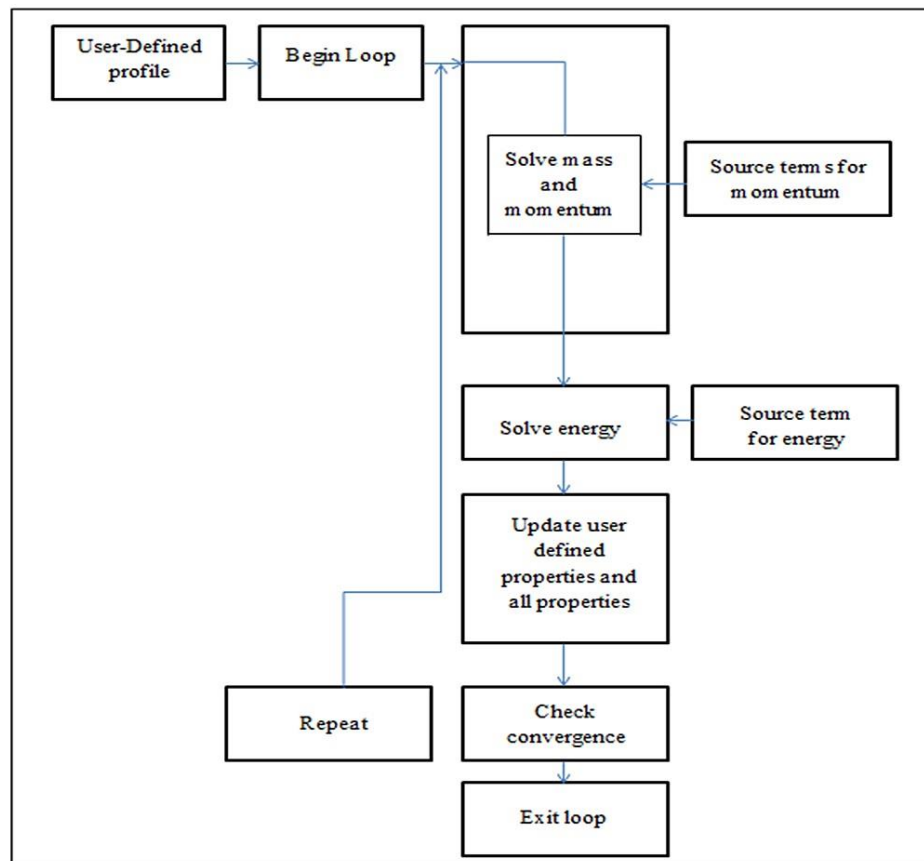
Figure 8. Schematic representation of the solution process.

In the second stage material attributes such as density, specific heat capacity andthermal conductivity are definedwith respect to temperature variable once the momentum and energy equations are established from theuser-defined functions. The mathematical equations are solved byPISO algorithm whereby momentum and energy conservation equations are discretized by 3rd order Monotone Upstream-centered Schemes Conservation laws and 2nd order Up-wind. The solver computes the governing equations thereafterconvergence test is carried out for each iteration and above procedure is carried out until the convergence is determined.

The experimental data considered in this work is presented in Table 3. The experimental results for the development of computational model is adapted from an independent literature [1]. The computational results are compared with the experimental data. Figure 9 to 13presentsnumerically computed temperature contours on the specimen surface corresponding to different current input. The temperature is indicated by the different colours as shown in the figures below.
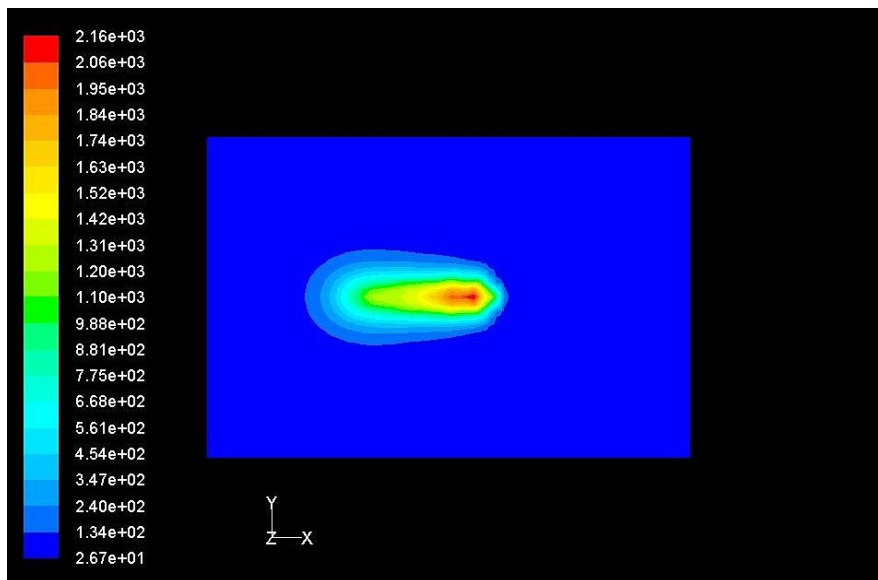

Figure 9. Temperature contour at 130A and speed 2mm/s.
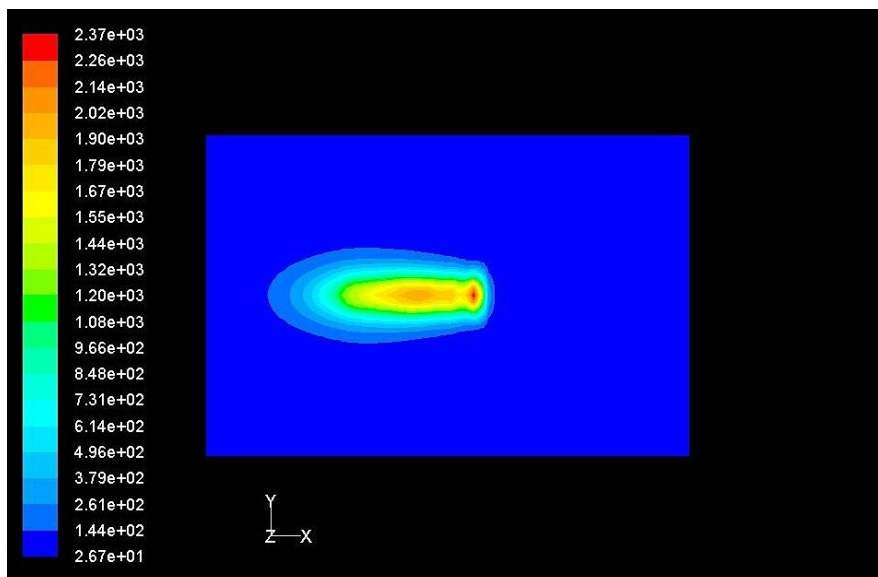
Figure 10. Temperature contour at 140A and speed 2mm/s.
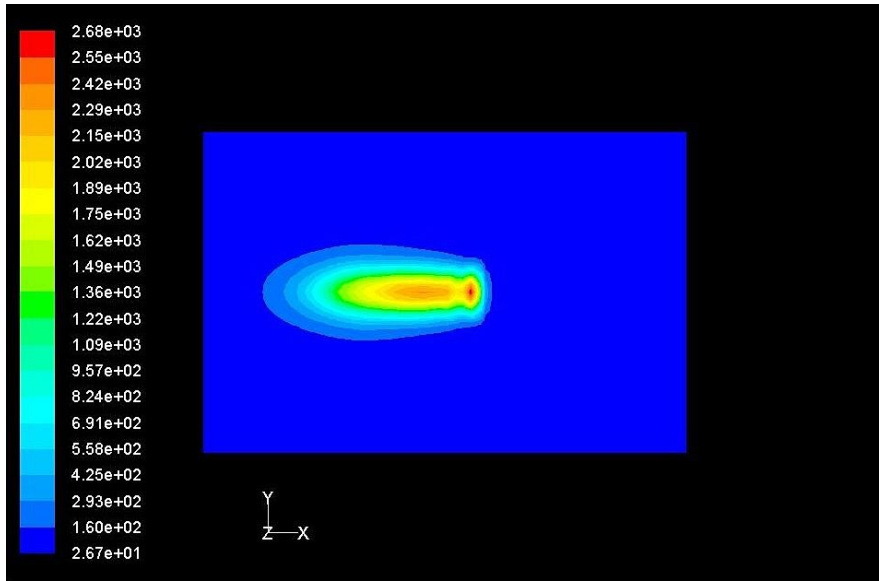
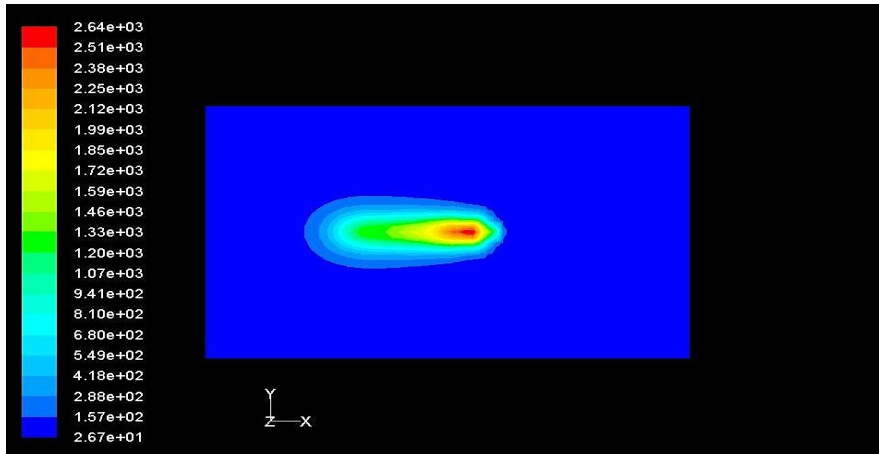Figure 11. Temperature contour at 150A and speed 2mm/s.

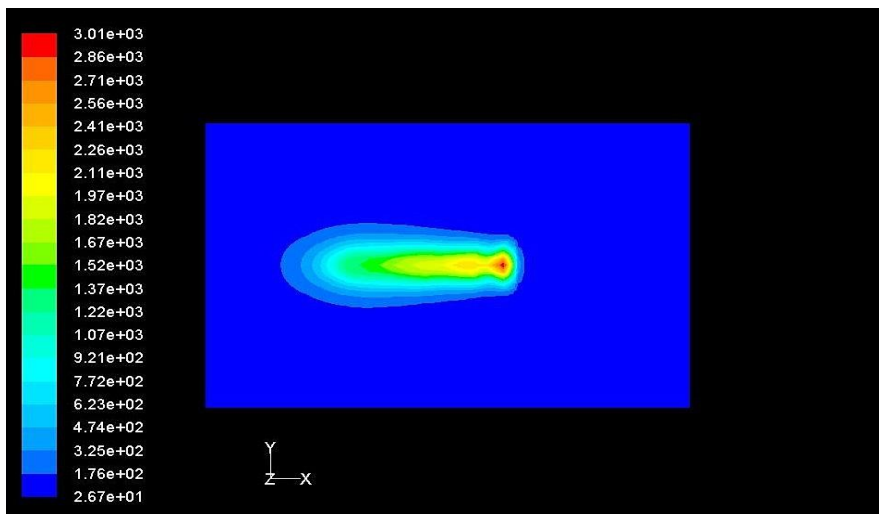Figure 12. Temperature contour at 140A and speed 3 mm/s.

Figure 13. Temperature contour at 140A and speed 4 mm/s.

45

Surface tension is a major parameterfor fluid transport in the melt pool when compared with electromagnetic and buoyancy forces. Generally flow of fluid is governed from smaller surface tension to higher surface tension. Usually higher the temperature of the surface lower will be the surface tension. Therefore, the fluid flows towards the melt pooledge on account ofreduced temperature. The maximum temperature is identified at the forepart section of the weldment which is the centerof the moving thermal model. The surface tension decreases as the penetration of the top surface increases and gradually the surface tension tends to disappear.

The melt pool is narrow and long due to moving heat source. The front part penetration is high but gradually it declines across the rear-endsection where solidification begins again from the lower section towards upper section.Figure 14 illustrates the flow of molten material and its zoom view can be observed in figure 15. The velocity tends to go higher when flow reaches the edge of the pool. Heat transfer takes place due to molten metal flow in the melt pool which is caused by surface tension factor. Due to little fluid flow inside the pool heat transfer gets highly weakened. The fluid flow directions are indicated by the arrow marks as demonstrated in the figure. The molten metal flow is more in the area where the heat source acts.
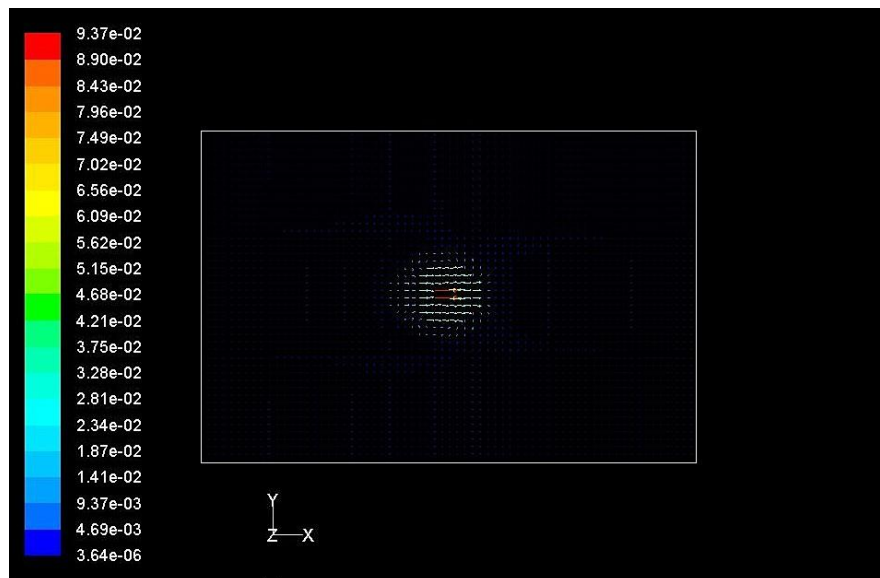

Figure 14. Fluid flow motion on the top surface of the specimen.
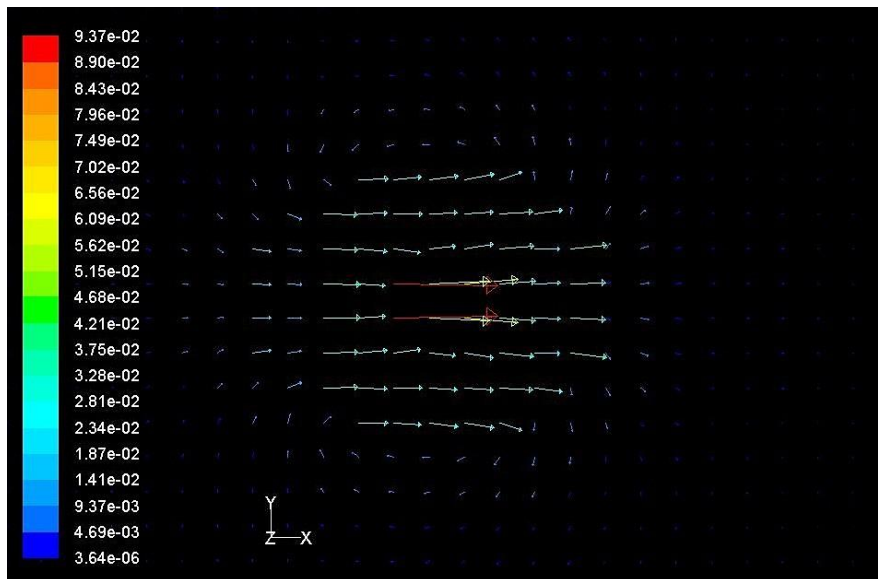
Figure 15. Zoomed view of fluid flow motion on the upper surface of the specimen.

The high velocity fluid flows forward and on the contrary low velocity fluid moves backward. The fluid flow motion is directed along the weld direction viz. positive X-axis at longitudinal plane. It strikes the solid parent metal domain or un-welded region and reverts backward. Along the depth of the melt pool, the magnitude of velocity vectors reduces gradually. The velocity vector magnitude is significant only up to half of the thickness of the specimen. This phenomena is due to the fact that the fluid flow transpires only up to the weld penetration.
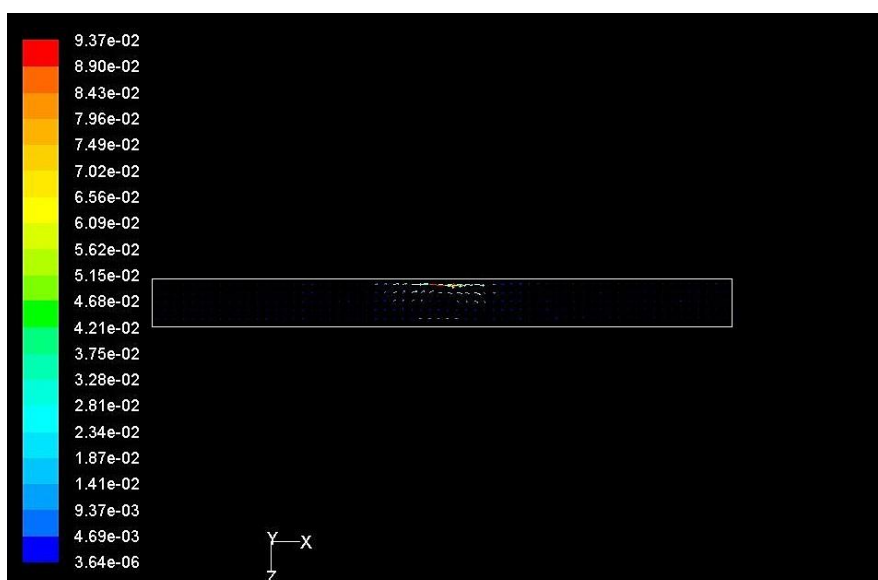

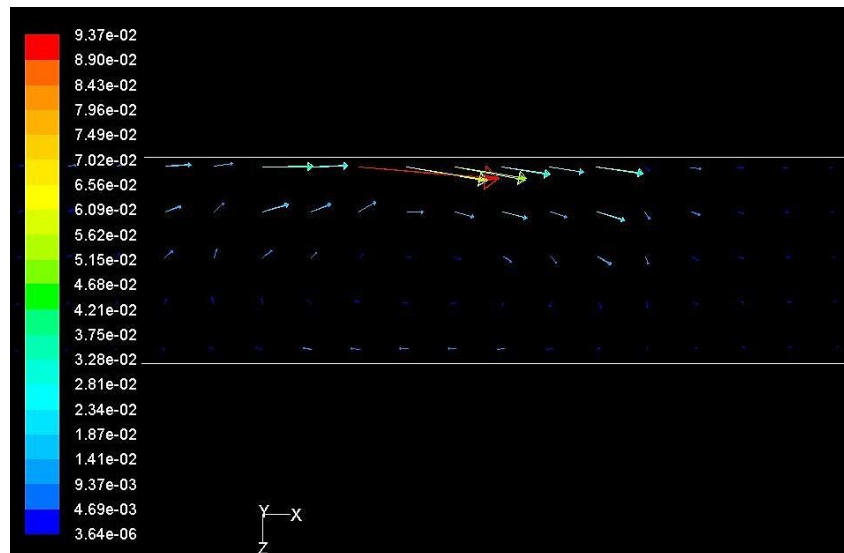Figure 16. Longitudinal view of fluid flow.

Figure 17. Zoomed view of fluid flow motion in X-axis direction.

As per the result the flow towards the inside of the weld pool decreases due to the velocity gradient. The reinforcement flow runs toward the molten pool and it is caused by the Marangoni force along the X-axis or welding direction (shown in figure 16 and 17). The arc prevails at a single location for few seconds at the initial stage to ensure the complete penetration and there is immediate transmission of heat to the surrounding. After a very short duration of time, specimen liquidustemperatureis attained and a tiny melt pool appearson the upper surface.The temperature goes down on the rear end of the specimen due to convection and radiation heat transmission process to the surrounding. Later the temperature falls down below the solidus temperature and melt pool starts solidifying. The highest temperature point in the melt pool moves along with the movement of thermal energy source. While the profile of melt pool remains same as the melt pool generates from initial point to end point.

To achieve dynamic equilibrium of heat transfer, pool extends rapidly.Melt pool tends to gradually decrease after reaching the equilibrium. After sometime when heat transfer reaches dynamic equilibrium the heat source moves at a constant speed as well as the pool moves at a uniform velocity and after that pool geometry hardly changes. Figure 18 shows the computed full penetration at welding speed 4 mm/s. Also, the gradual increase of the penetration with time can be observed in figure 19.
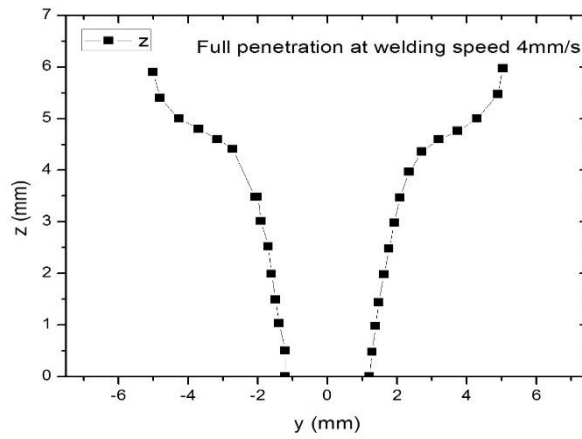
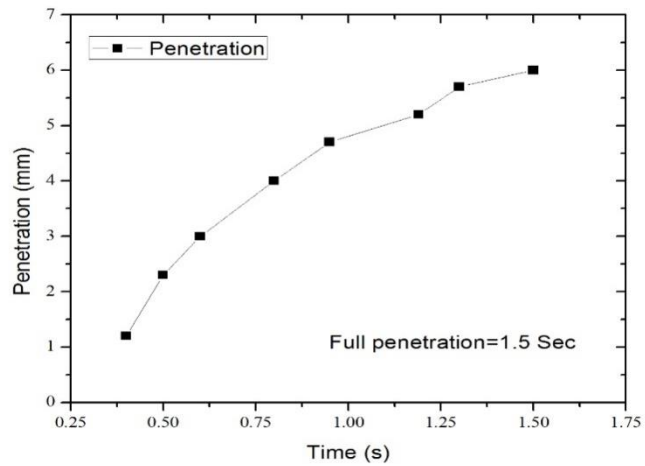Figure 18. Graphical representation of the penetration at welding speed 4mm/s.

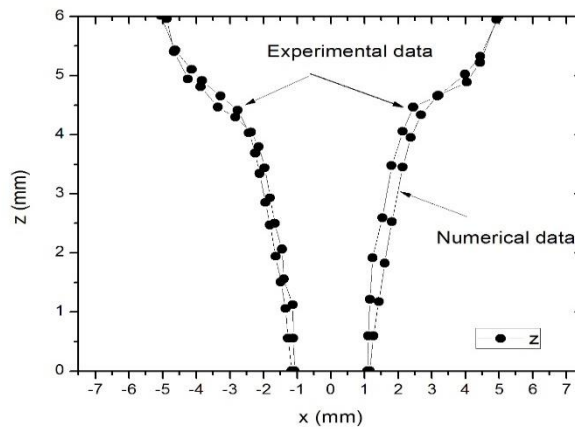

Figure 19. Penetration Vs time

Figure 20. Comparison between experimental and numerical data

The heat transfer from the upper region to lower regionin the melt pool is by convection and for the solid metal it is by conduction mode. The melt area at the lower surface is much lower than the upper surface which is obvious. From numerical result, maximum width of the top surface is 9.9mm which is very near to the experimental data i.e. 9.84mm. The maximum width of the bottom surface from numerical estimation is 2.3mm while that of experimental data is 2.2 mm which is infact quite close. From figure 20, it can be recognised that a fair agreement is established between computationaland experimental data.The numerical results states that arc power increases along with welding current and voltage. For the first case keyhole is not formed at 130A and 19.8 V. When welding current is increased to 140 A and voltage to 21.5V full penetration is recognised. Moreover, with an increase in weld parameters, melt pool area started getting larger. Although, if it exceeds high plasma arc pressure the strength of the specimen declines after the melting and solidificationprocess. Based on results it can be recognized that plasma arc power is optimal in between 1 W and 2 W andthe penetration is fully optimized at 1.5 seconds.

CONCLUSION AND FUTURE SCOPE

Based on the present work with reference to the thermal transmissionanalysis and flow behavior during PAW process, the following conclusions may be drawn along with future scope of the work.

- Due to the arc voltage and current the specimen partially penetrated by the arc and the penetration gradually increases when speed and voltage are increasing.Depth of penetration is highest at the speed of 17.5 m/s, 425A and 28.5V.

- Numerical analysis is done in Plasma arc welding to study the heat transmission process and molten metal flow analysis in weld pool.Computed results are compared with the experimentally measure values of independent literature.

- From numerical result, maximum width of the top surface is 10mm which is very near to the experimental data i.e. 9.84mm.The maximum width of the bottom surface as per numerical results 2.32mm, closed to experimental data 2.2 mm.Keyhole is formed during welding at 1.5 sec.

The keyhole wall is maintained bythe liquid gas interfacial state andthe keyhole characteristics is governed by the thermal energy and force balance. Infact the keyhole

stability is the most vital concept although there is no accurate definition and evaluation strategy to comprehend the PAW process.

References

1. C. S. Wu, T. Zhang and Y. H. Feng: Numerical analysis of the heat and fluid flow in a weld pool with a dynamic keyhole, *International Journal of Heat and Fluid Flow,* **40**, 2013, 186–197.

2. Yan li, YanhuiFeng, Xinxin Zhang, Chuansong Wu; Energy propagation in Plasma arc welding With keyhole tracking, *Energy*, **64**, 2004, 1044-1056.

3. D. Rosenthal, The theory of moving sources of heat and its application to metal Treatments, *Trans. ASME* 43, 11, 849-865, 1946.

4. R.R. Rykalin, Energy sources for welding, *Weld. World*, 12, 227-248, 1974.

5. E. Friedman, Analysis of weld puddle distortion and its effect on penetration, *Weld. J. Res. Suppl.* 57, 161-166, 1978.

6. G.W. Krutz, L.J. Segerlind, Finite element analysis of welded structure, *Weld. J. Res. Suppl.* 57, 211-216, 1978.

7. Goldak, J., Chakravarti A. and Bibby. M, A new finite clement model for welding heat sources", *Metall. Trans.* 15(6), 299-305, 1984.

8. C.S. Wu, T. Zhang and Y.H. Feng, Numerical analysis of the heat and fluid flow in a weld pool with a dynamic keyhole*, International Journal of Heat and Fluid Flow* 40,186–197, 2013.

9. Yan Li , Yan-Hui Feng , Xin-Xin Zhang ,Chuan-Song Wu, An improved simulation of heat transfer and fluid flow in plasma arc welding with modified heat source model,*International Journal of Thermal Sciences*, 64, 93-104, 2013.

10. C.S. Wu, H.G. Wang, Y.M. Zhang, A new heat source model for keyhole plasma arc welding in FEM analysis of the temperature profile, *Weld. Journal* 85 284-291. 2006.

11. Li, T.Q., Wu, C.S., Feng, Y.H., Zhang, L.C., Modeling of the thermal fluid flow and keyhole shape in stationary plasma arc welding, *International Journal of Heat Fluid Fl* 34, 117–125 2012.

12. C.S. Wu, Q.X. Hu, J.Q. Gao, An adaptive heat source model for finite-element analysis of keyhole plasma arc welding,*Comput. Mater. Sci.* 46 167e172. 2009.

13. T.Q. Li , C.S. Wu, Y.H. Feng, L.C. Zheng: Modeling of the thermal fluid flow and keyhole shape in stationary plasma arc welding,*International Journal of Heat and FluidFlow,* 34,2012, 117–125.

14. C.S.Wu, W.Zheng and M.A.Chen: Improving the prediction accuracy of Keyhole establishment time in plasma arc welding, *Numerical heat transfer, PART A,* 66, 2014, 420-432.

15. T.Q.Li, C.S. Wu, J. Chen: Transient variation of arc heat flux and pressure distribution on keyhole wall in PAW, *Weld world*, 60,2016,363-371.

16. N. Yadaiah & S. Bag & C. P. Paul & L. M. Kukreja; Influence of self-protective atmosphere in fiber laser welding of austenitic stainless steel, *International Journal of Advanced Manufacturing Technology;* 86(1), 2016, 853–870.

17. Wu CS,Wang HG, ZhangYMA; New heat source model for keyhole plasma arc welding in fem analysis of the temperature profile, Weld Journal 2006, 284–291.

18. Yan Li , Yan-Hui Feng , Xin-Xin Zhang and Chuan-Song Wu, An improved simulation of heat transfer and fluid flow in plasma arc welding with modified heat source model, *International Journal of Thermal Sciences* 64, 93-104, 2013.